Forecasting tropical cyclone tracks in the Northwest Pacific based on a deep-learning model

Liang Wang[1,2], Bingcheng Wan[3], Shaohui Zhou[3], Haofei Sun[1,2], Zhiqiu Gao[1,3*]

[1] State Key Laboratory of Atmospheric Boundary Layer Physics and Atmospheric Chemistry, Institute of Atmospheric Physics, Chinese Academy of Sciences, Beijing, 100029, China

[2] University of Chinese Academy of Sciences, Beijing, 100049, China

[3] School of Atmospheric Physics, Nanjing University of Information Science and Technology, Nanjing, 210044, China

Correspondence to: Dr. Zhiqiu Gao(zgao@mail.iap.ac.cn)

Abstract. Tropical cyclones (TCs) are one of the most severe meteorological disasters, making rapid and accurate track forecasts crucial for disaster prevention and mitigation. Because TC tracks are affected by various factors (the steering flow, thermal structure of the underlying surface, and atmospheric circulation), their trajectories present highly complex nonlinear behavior. Deep learning has many advantages in simulating nonlinear systems. In this paper, we explore the movement of TCs in the Northwest Pacific from 1979 to 2021 based on deep-learning technology, divided into training (1979–2014), validation (2015–2018), and test sets (2019–2021), and create 6–72 h TC track forecasts. Only historical trajectory data are used as input for evaluating the forecasts of the three recurrent neural networks utilized: recurrent neural network (RNN), long short-term memory (LSTM), and gated recurrent unit (GRU) models. The GRU approach performed best; to further improve forecast accuracy, a model combining GRU and a convolutional neural network (CNN) called GRU_CNN is proposed to capture the characteristics varying with time. By adding reanalysis data of the steering flow, sea-surface temperatures, and geopotential height around the cyclone, we can extract sufficient information on the historical trajectory features and three-dimensional spatial features. The results show that GRU_CNN outperforms other deep-learning models without CNN layers. Furthermore, by analyzing three additional environmental factors through control experiments, it can be concluded that the historical steering flow of TCs plays a key role, especially for short-term predictions within 24 h, while sea-surface temperatures and geopotential height can gradually improve the 24–72-h forecast.

28 The average distance errors at 6 h and 12 h are 17.22 km and 43.90 km, respectively. Compared with

29 the 6-h and 12-h forecast results (27.57km and 59.09km) of the Central Meteorological Observatory,

30 the model proposed herein is suitable for short-term forecasting of TC tracks.

31 **1 Introduction**

32 The Northwest Pacific is the most active basin for tropical cyclones (TCs) in the world, generating over

33 one-third of the total number of TCs (Gray, 1968). China, located on the western side of the Pacific

34 Ocean with a coastline longer than 18,000 km, is one of the countries most severely influenced by TCs.

35 These storm systems are accompanied by strong winds, heavy precipitation, and storm surges, resulting

36 in severe disasters that affect human lives and economic growth (Goldenberg et al., 2001). Studies have

37 shown that global warming will progressively intensify TCs over time (Emanuel, 2017; Schulthess et

38 al., 2019). Since disasters caused by TCs are unavoidable and potentially destructive, accurately

39 predicting the movement of TCs can provide sufficient preparation time for people in affected areas to

40 implement disaster mitigation strategies.

41 Given the uncertainty of TC movements, the complexity and nonlinearity inherent in the

42 atmospheric system, and the scarcity of ocean-based observational data, accurately predicting the

43 center positions and intensities of TCs is a challenge. Currently, forecasting methods for TCs are

44 mainly divided into two categories, with the primary method being numerical weather prediction

45 (NWP). NWP calculates the approximate solution of partial differential equations involving

46 atmospheric state variables when the initial conditions and boundary conditions of the atmosphere are

47 known. In this way, some elements, such as the tracks and intensities of the TCs, can be solved

48 iteratively; GRAPES-TYM (CMA), GFS (NCEP), and IFS (ECWMF) are the main NWP models.

49 Although these model forecasts can provide accurate results, there are limitations in methods relying on

50 high-performance computers and requiring ~~numerous calculations, accurate mathematical descriptions~~

51 ~~of physical atmospheric mechanisms, and~~ precise initial conditions. At the same time, ensemble

52 forecast methods (GRAPES-GEFS, ECMWF-EPS, NCEP-GEFS) have been used to reduce the

53 influence of various uncertainties on the numerical prediction results (Goerss, 2000). The other

54 forecasting method is a statistical model, which generally utilizes multiple regression. The statistical

55 model is mainly based on the relationship between the movement of the TC and its specific historical

characteristics, but it usually does not consider any physical processes. The National Hurricane Center has successively adopted statistical models such as NHC64 (taking observational data and historical 12h movements as factors), NHC67 (increasing factors based on NHC64), CLIPER (climate persistence factors) (Neumann and Hope, 1972), and NHC72 (a combination of NHC67 and CLIPER). Most traditional TC statistical models adopt a linear regression model, and it is difficult for this approach to address the nonlinear problems in TC track forecasting (Roy and Kovordányi, 2012). At the same time, manual feature selection is unable to produce accurate predictions. CLP5 had the largest Mean absolute error(MAE) of all models for TCs occurring from the Eastern Pacific and North Atlantic (Boussioux et al., 2022). Li-Min et al. (2009) used the BP neural network to predict that the average distance error of the 6h movement track of six typhoons in 2005 improved by 36.9km, compared with CLIPER.

Deep learning is an emerging application of supercomputing that is continuously being developed; many researchers have tried to adopt this technology to forecast weather and meteorological elements, including visibility (Ortega et al., 2022), wind speeds (Liu et al., 2018), radar echoes (Klein et al., 2015), and precipitation nowcasting (Shi et al., 2015). Deep learning is a statistical model that solves nonlinear and complex relationships from historical sample data based on neural network algorithms. The weight factor between network nodes is automatically adjusted through repeated training; thus, neural network algorithms have the advantages of strong adaptability and fault tolerance. TCs have complex dynamic mechanisms and are easily affected by many factors, including environmental steering flow, Beta effects, underlying surface conditions, the asymmetric structure of the inner core, and mesoscale circulations (Chan and Kepert, 2010). Artificial neural networks (ANNs) have been applied to predict TC tracks due to their strong learning ability and advantages in simulating nonlinear systems. Until the 2010s, ANN and back propagation (BP) networks were the mainstream neural network methods for forecasting TC tracks (Ali et al., 2007; Li-Min et al., 2009; Wang et al., 2011). Since the mid-2010s, more new methods have been introduced into TC prediction due to the development of deep-learning technology. Recurrent neural networks (RNNs) are suitable for TC track forecasting owing to their ability to handle time series data of arbitrary lengths. Moradi Kordmahalleh et al. (2015) applied a sparse RNN to Atlantic hurricane trajectory prediction using the dynamic time warping (DTW) method to measure the hurricane most similar to the target hurricane for training. Gao

et al. (2018) used long short-term memory (LSTM) to predict typhoon tracks in the Northwest Pacific Ocean; the ratio of the cyclone training set and test set was set at 8:2, and the 24-h prediction error could reach 105 km. Alemany et al. (2018) proposed an RNN based on a grid system to predict hurricanes in the Atlantic, potentially improving the 6-h prediction accuracy with a root mean square error (RMSE) of 0.11 for the test set. Kim et al. (2018) performed a TC identification task based on ConvLSTM to train WRF-simulated data, and the results are significantly better than those of a convolutional neural network (CNN) and the results show the average precision of the forecast was improved by 78.99% than those of a convolutional neural network (CNN). These CNNs have attracted attention given their suitability for processing 2D image data; they maintain spatial correlations by implementing convolution layers and then pooling layers for feature extraction. Giffard-Roisin et al. (2020) combined historical trajectory data with wind field reanalysis data as input to a CNN and predicted Atlantic hurricane tracks since 1979, with an average error of 32.9 km for 6-h predictions.

Making full use of different types of data is essential for deep learning. TC-related data are mainly divided into the following three categories: observational trajectory data, remote sensing data, and meteorological reanalysis field data. A multi-modal approach enables more accurate predictions than an approach using a single data source does. Zhang et al. (2018) developed a matrix neural network (MNN) model that preserves the spatial information of the TC tracks, and it has demonstrated the ability to provide more accurate results compared with other models (GRU, LSTM, Multi-Layer Perceptron, and RNN). Ruttgers et al. (2019) built generation adversarial networks (GANs) adding satellite images to predict the coordinates of the typhoon center and generate cloud maps of future typhoons. Liu et al. (2022) proposed a new deep learning–based model, DBFNet, to effectively fuse the inherent features of cyclones and reanalyze 2D pressure field data. PreviousAbove studies have shown that deep-learning models that incorporate multiple data types can improve the track forecast of TCs to a certain extent. Still, most of them have neglected to describe and analyze the meteorological factors that affect the movement of TCs, ignoring valuable features. The 6-hour average distance error between predicted and real location by the fusion network (wind+track) is 32.9 km, while the network prediction results without adding wind variables are 35km (Giffard-Roisin et al., 2018)., which indicates that the addition of meteorological field variables can effectively improve the prediction accuracy.

114   ~~Therefore, in t~~This paper _attempts to_~~, we~~ propose a new method for TC track prediction based on

115   a combination of CNN and GRU models that incorporate data regarding the trajectory, steering airflow,

116   sea-surface temperatures, and geopotential height as input features, aiming to improve the accuracy of

117   TC track forecasts by leveraging big data. The main contents of this paper are as follows: Section 2

118   introduces the necessary data and _and data preprocessing_~~methodology principles~~. Section 3 describes

119   the experimental design and the framework of the fusion model (GRU_CNN) proposed in this paper.

120   Section 4 presents the experimental results and comparative analysis, and Section 5 provides a

121   summary and discussion of shortcomings and directions for future work.

122   **2 Data _and data preprocessing_~~and methods~~**

123   **2.1 Data**

124   The data used in this paper are trajectory data and reanalysis environmental data. The TC track data

125   come from the International Best Track Archive for Climate Stewardship (IBTrACS), which

126   encompasses all TCs globally. For each TC, the latitude, longitude, central pressure, maximum wind

127   speed, direction, moving speed, and other data are recorded at 3-h intervals. The IBTrACS dataset

128   contains data from different basins where cyclones show different characteristics; thus, this paper only

129   selects TCs that occur in the Northwest Pacific Ocean. To better mine the hidden information, the 2D

130   cyclone track data were chosen according to the method proposed by Li-Min et al. (2009), and 19

131   movement characteristics were obtained, including the past 24-h longitude, latitude, central

132   atmospheric pressure, maximum wind speed, meridional moving speed, zonal moving speed, moving

133   direction/speed, the difference between those values and those at the current time, and the angle, zonal

134   distance, and meridional distance formed between the data over the past 24 h and in the present

135   moment. _Because they are influenced by the earth's rotation, TCs will be biased to the northwest_

136   _(Kitade, 1981). The Coriolis parameters corresponding to the latitude of the TCs in the past 24 hours_

137   _are also included_~~In addition, the Coriolis parameter corresponding to the latitude of the past 24 h~~

138   ~~influences the geostrophic deflection force on the TCs.~~_._

139   Both observational and theoretical studies have shown that TC movement is closely related to

140   large-scale airflow fields (Holland, 1983), and TC movement is mainly affected by the steering flow

141 (Brand et al., 1981; Chan, 1984). ~~Because they are influenced by the earth's rotation, TCs will be~~

142 ~~biased to the northwest (Kitade, 1981).~~ Interactions among weather systems, the subtropical

143 anticyclone, Westerlies, and the Tibetan High will also affect the movement of cyclones (George and

144 Gray, 1976; Chan et al., 1980).

145   The geopotential heights of 300 hpa, 500 hpa, and 700 hpa are selected as the locations for the

146 high, middle, and low-level circulation data, respectively. In addition, the underlying surface conditions

147 must be considered, and, in the case of a weak guidance environment, TCs tend to move toward

148 warmer sea-surface temperatures (Sun et al., 2017; Katsube and Inatsu, 2016). Meteorological

149 environmental data are obtained by downloading high-resolution ERA5 reanalysis data from the

150 European Centre for Medium-Range Forecasting (ECMWF). Holland (1984) noted that the deep mean

151 circulation from 850 hpa to 300 hpa can better represent the direction of a TC. Therefore, the

152 environmental data for the preceding 24 h were extracted as follows:

153 (1) The u- and v-component data of the wind field on the four isobaric surfaces (300 hpa, 500 hpa, 700

154 hpa, 850 hpa): Centered the TC, extend 10 degrees outward in the zonal and meridian direction

155 respectively. ~~A 10° radius is extended from the center of the TC.~~ Since the resolution of the selected

156 reanalysis data is $1° \times 1°$, a 21×21 grid can be formed.

157 (2) The sea-surface temperature (SST): 10 degrees outward in the zonal and meridian direction i~~A 10°~~

158 ~~radius i~~s again extended from the TC center to form a 21×21 grid.

159 (3) The geopotential heights of 300 hpa, 500 hpa, and 700 hpa: A grid is extended $+35°$ to the north,

160 $-10°$ to the south, $-40°$ to the west, and $+40°$ to the east from the center of the TC, forming a 46×81

161 grid.

162 **2.2 Data preprossesing**

163 2.2.1 Devortexing

164 Because the actual weather circulation is very complex and includes information about the TC itself,

165 the surrounding airflow, and the interaction between the two, it is necessary to separate the cyclone

166 vortex from the surrounding airflow to obtain the steering flow. The most commonly used method

167 (Lownam, 2001; Galarneau and Davis, 2013) corrects the vorticity and divergence by solving the

168 change in the velocity stream and potential functions, respectively, and then calculates the modified

velocity field. The modified flow field can be interpreted as having a non-rotating wind and non-diverging wind. There must be potential velocity in the irrotational motion and a stream function in the non-divergent motion. The relationship between them can be expressed as follows:

$$\nabla^2 \psi = \zeta \tag{1}$$

$$v_\psi = \hat{k} \times \nabla \psi \tag{2}$$

Where ψ is the stream function without divergence, ζ is the relative vorticity, and v_ψ is the non-divergent wind (rotating wind). To define the rotating wind, the vorticity outside the vortex radius is set to zero, and $\psi = 0$ is specified on the horizontal boundary. The iterative relaxation method is used to solve the stream function of Eq. (1) at all layers and then to calculate v_ψ using Eq. (2). In the case of divergence, Eqs. (1) and (2) are replaced by:

$$\nabla^2 \chi = \delta \tag{3}$$

$$v_\chi = \nabla \chi \tag{4}$$

Where χ is the potential velocity, δ is the divergence, and v_χ is the non-vorticity wind. The divergence outside the vortex radius is set to zero and the potential function $\chi = 0$ on the boundary of the region. The velocity potential can be solved in the same manner to calculate v_χ. The ambient wind field with the vortex removed can be obtained by subtracting the rotating wind and divergent wind from the original wind field, V:

$$v_{env}(x, y, p) = V(x, y, p) - v_\chi(x, y, p) - v_\psi(x, y, p) \tag{5}$$

2.2 Methods

2.2.2 Random forest

By sorting features based on importance, random forest selects the best feature combination and reduces the input feature dimensions Selecting features based on importance is a fundamental step in machine learning that most efficiently directs variables for machine learning models (Díaz-Uriarte and Alvarez De Andrés, 2006; Genuer et al., 2010). Random forest is a supervised learning method that selects the best feature combination and reduces the input feature dimension. The random forest contains N decision trees, and N is generally set to 100. Since bootstrapping (random sampling with

replacement) is used to generate the random decision tree, all samples are not in the generation process of a tree, and the unused samples are called "out-of-bag" (OOB) samples. Through OOB samples, the accuracy of this tree can be evaluated. , and it is usually calculated via the following four steps:

Select the OOB data and calculate the OOB data error:

$$error = \frac{1}{n} \sum_{i=1}^{n} (f_i - y_i)^2$$

f_i: predicted value, y_i: actual value, n: number of samples (1/3 of the total).

Randomly add noise interference to the features of all samples of the OOB data and calculate the OOB data error ($error^m$) again.

$$error^m = \frac{1}{n} \sum_{i=1}^{n} (f_i^m - y_i)^2$$

f_m: Predicted value after adding noise to feature m.

Calculate the importance I of all features.

$$I = \frac{1}{N} \sum_{j=1}^{N} (error_j^m - error_j)$$

N: the number of decision trees, $error_j$: OOB data error, $error_j^m$: OOB data error after adding noise.

According to the order of feature importance, delete the features with less importance in turn, repeat the above three steps, calculate the OOB data error, and select the combination with the lowest error.

The OOB score represents the score of the model performance:

$$R = 1 - \frac{\sum_{i=1}^{n} (f_i - y_i)^2}{\sum_{i=1}^{n} (y_i - \hat{y})^2}$$

$$OOB_{score} = \frac{1}{N} \sum_{j=1}^{N} R_j$$

Before model training, it is necessary to determine whether the 19 trajectory features all have an impact on the prediction results. Figure 1(a) shows the long name corresponding to the short name of 19 input features and Figure 1(b) shows the 19 features' order of importance calculated using the random forest. For forecasting the difference in longitude and latitude within the following 72 hours, characteristics like the historic longitude or the angle formed by the historical moment and the current moment are

218 significant. The decision about whether to exclude some less important features, however, requires

219 further consideration. ~~Based on Eq. (9) and Eq. (10), t~~The OOB scores under different input feature

220 dimensions are computed, with variables input in the order of importance, as shown in Fig. 1(c). In the

221 case in which the first 11 features are sorted by importance, the OOB score is the highest, and the

222 features added later will no longer affect the result; in other words, the best combination is that of the

223 first 11 features.

224

225
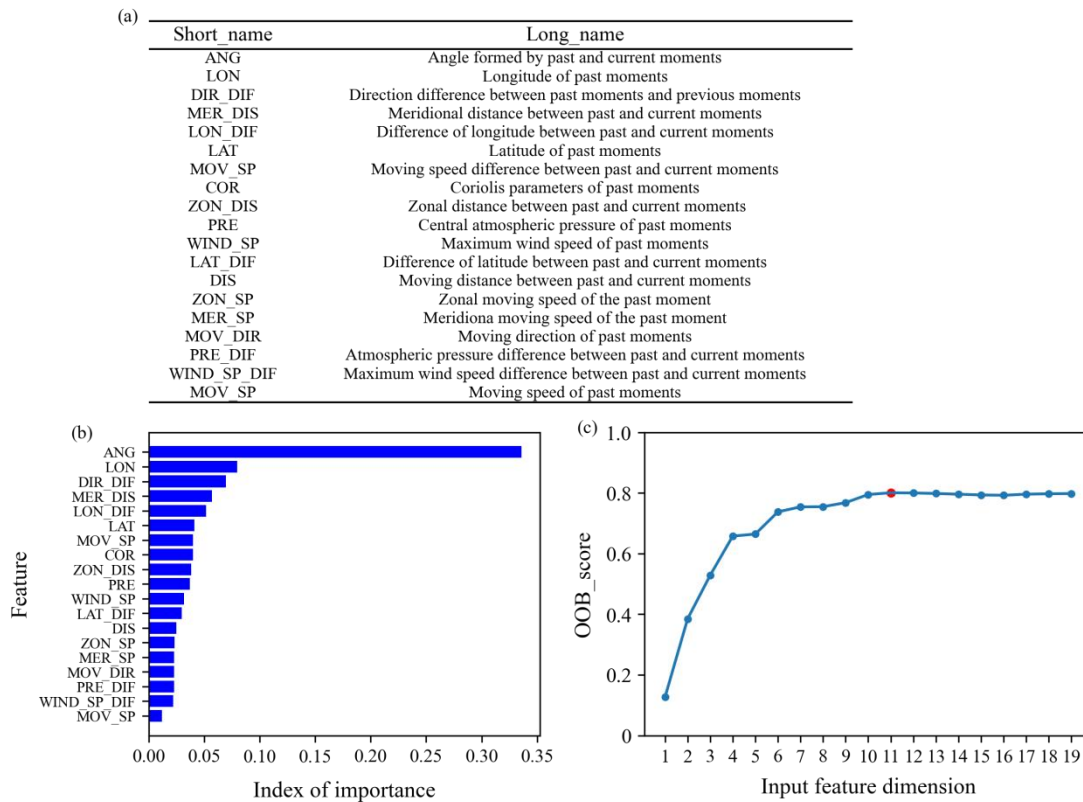
226 **Figure 1: (a) Table displaying the short and long names of features, (b) the importance index of features,**

227 **and (c) the OOB_score of different feature combinations based on the random forest (red dot indicates the**

228 **maximum**

229 **value).**

230
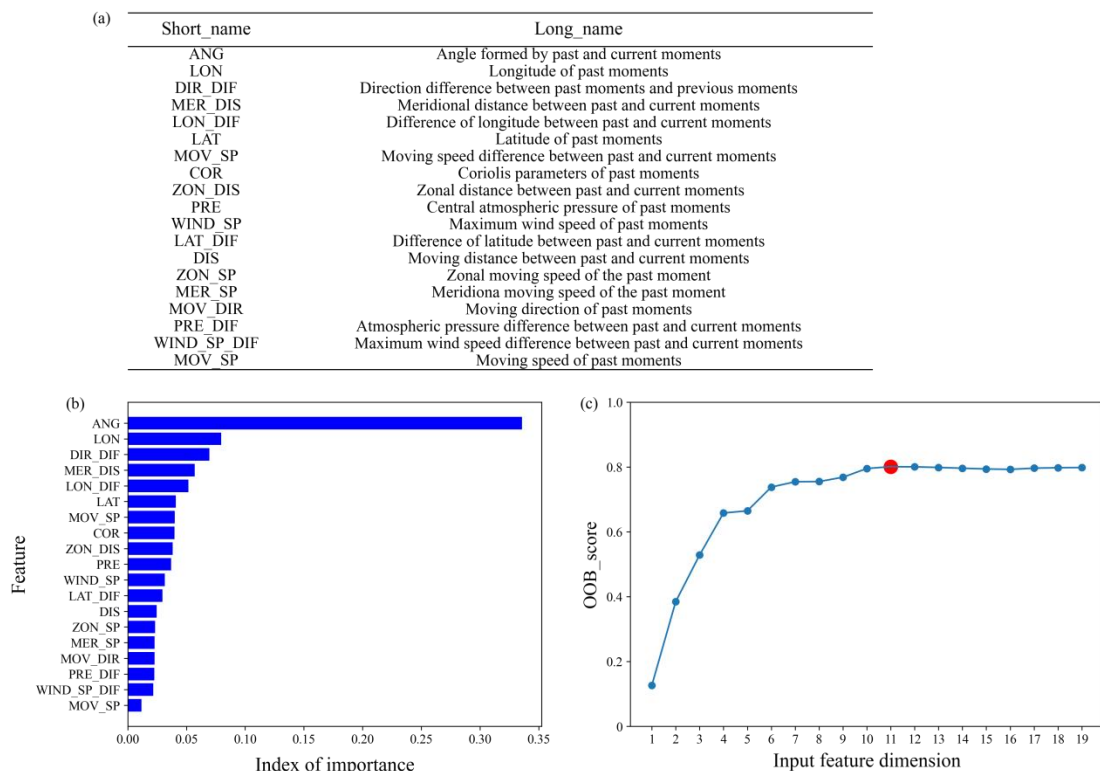
3 Experiment

3.1 Experimental design

233 Our goal is to predict the TC movements for the following 6–72 h using the trajectory data and

234 surrounding environmental field from the previous 24 h. We explore TC movement in the Northwest

235 Pacific from 1979 to 2021 and consider the longitudinal and latitudinal changes in the following 6–72 h

236 as the quantitative prediction variables, with the center of the TC at the current time as the reference

237 point. Since the maximum forecast hour is 72 and the input sequence time length is 24 h, TCs that

238 persist for longer than 96 hours are removed. All samples obtained based on the sliding window of the

239 input-prediction sequence length are divided into three groups in chronological order: training set

240 (1979–2014), validation set (2015–2018), and test set (2019–2021). There are 36473 samples, of which

241 90% are trained, and the remaining 10% are validated; 49 TCs from 2019 to 2021 are used for testing,

242 and the number of test samples is 2095.

3.2 Model framework

23.2.1 Recurrent Neural Network

RNNs can process sequences of any length using neurons with self-feedback, characterized by architectural features intentionally designed to preserve historical information, showing a remarkable ability to process sequential data. (Graves et al., 2013) (Bathla, 2020) (Wang and Fu, 2020). However, simple RNNs have difficulty in dealing with the long-term dependence of the sequence; when the sequence length exceeds a certain threshold, the information may disappear during the transmission process, resulting in large deviations in prediction accuracy. The LSTM network proposed by Hochreiter and Schmidhuber (1997) can avoid the gradient disappearance and explosion phenomena that occur in the standard RNN. While GRU (Cho et al., 2014) is an improved and optimized neural network based on LSTM, it has a faster convergence speed and maintains accuracy levels close to those of LSTM.

23.2.2 Convolutional Neural Network

CNN can extract features automatically by processing the input patterns and translating the same convolution kernel from top to bottom and from left to right. The spatial relationship is fixed with the distribution of neurons, and the local connection and weight sharing of neurons reduce the training complexity by reducing the number of parameters. Lecun et al. (1998) first used CNN for handwritten character recognition with average pooling and the tanh activation function. Krizhevsky et al. (2012) proposed the AlexNet model in the ImageNet competition, using the ReLU function instead of the traditional tanh function to introduce nonlinearity and solve the gradient disappearance problem of the activation function when the network was relatively deep, employing maximum pooling to avoid the blurring effect of average pooling. Ioffe and Szegedy (2015) applied batch normalization to image classification models, which significantly accelerated the training of deep networks, and batch normalization helped alleviate the problem of gradient exploding or vanishing.

267 **23.2.3 GRU_CNN**

268 Due to differences in the data sources, a new model must be developed to integrate the four

269 information sources into the neural network using the Keras deep-learning framework. The specific

270 model structure is shown in Fig. 3. For the 3D meteorological data, the data are superimposed on the

271 geopotential height (pressure level), so the input data for the CNN consist of multiple two-dimensional

272 matrices. the gray filling arrow represents the TimeDistributed layer that is applied to a series of

273 tensors in the processing of the time dimension~~The TimeDistributed layer is applied to a series of~~

274 ~~tensors in the processing of the time dimension~~. In addition, the CNN adopts a typical architecture with

275 alternating convolution layers (Conv layers) and maximum pooling layers (Maxpool layers), The black

276 solid arrow means the Flatten layer converting two-dimensional data into one-dimensional vectors at

277 the end of the CNN network and ~~eventually creating a fully connected layer~~the dashed black arrow

278 represents the fully connected layer in the network framework. All hidden layers are equipped with

279 batch normalization, and this paper employs ReLU as the activation function.

280 For the two-dimensional trajectory data of the TCs, x_i^j represents the input value of the ith feature

281 at the jth timestamp, $i \in (1, n)$, $j \in (1, t)$, and they are input into GRU. The model is based on the Adam

282 optimizer and trained with the RMSE between the forecast and the actual value as a loss function. Due

283 to the different properties among the wind field, pressure field, SSTs, and past trajectory data, different

284 learning rates are required for the neural network. Therefore, the parameters of each branch in the

285 model can be trained with the same task, and then the branches can be fused into one network (Concat

286 layer)~~,~~, that is, the dashed red arrow means the merging of multiple vectors into one vector. It is

287 eventually ~~and~~ stitched with output with a fully connected layer ; thereafter, the parameters can be

288 adjusted slightly. Table 1 lists the input and output size of each layer in the network framework,

289 including convolution kernel size, stride, and channel number.
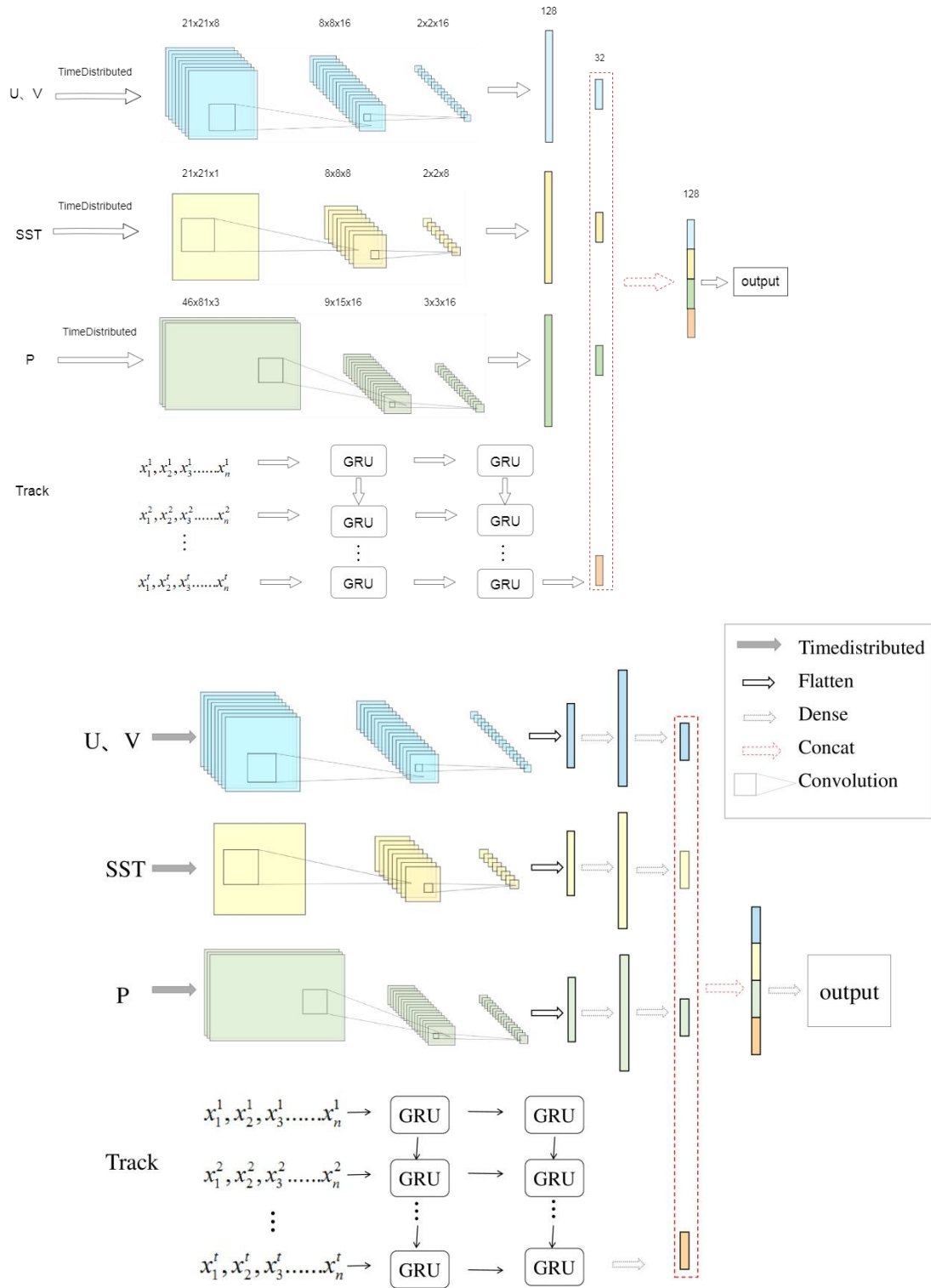
Figure 233: The model framework and network structure of GRU_CNN.

Table 1 Each layer architecture of the GRU_CNN

Layers	Kernel Size	Stride	Channel	Input Size	Output Size

Conv_uv	7×7	2	8	21×21	8×8
MaxPool_uv	4×4	4	16	8×8	2×2
Flatten__uv	-	-	16	2×2	64
Dense_uv_1	-	-	-	64	128
Dense_uv_2	-	-	-	128	32
Conv_sst	7×7	2	1	21×21	8×8
MaxPool_sst	4×4	4	8	8×8	2×2
Flatten_sst	-	-	8	2×2	32
Dense_sst_1	-	-	-	32	128
Dense_sst_2	-	-	-	128	32
Conv_p	14×25	4	3	46×81	9×15
MaxPool_p	5x11	4	16	9×15	2×2
Flatten__p	-	-	16	2×2	64
Dense_p_1	-	-	-	64	128
Dense_p_2	-	-	-	128	32
GRU_1	-	-	-	8×11	8×128
GRU_2	-	-	-	8×128	128
Dense_GRU	-	-	-	128	32
Concat_layer	-	-	-	-	128

3.3 Data normalization

The differences in the dimensions of the input data will cause a variable with a larger value to have a more significant impact on the model. Therefore, it is necessary to normalize the data before model training to map the input data from 0 to 1. To eliminate the influence of different dimensions on the model, the original value x is normalized as x':

$$x' = \frac{x - x_{min}}{x_{max} - x_{min}}$$

Where x_{max} and x_{min} are the maximum and minimum values of the variable x, respectively.

3.4 Evaluation criteria

RMSE is the root mean square error obtained by calculating the predicted value P_i and the observed value O_i. The formula is as follows:

$$RMSE = \sqrt{\dfrac{\sum\limits_{i=1}^{n}(P_i - O_i)^2}{n}}$$

~~Since the latitude and longitude represent different spatial distances in kilometers, when comparing~~

~~other models, the distance error (Dis) is calculated in kilometers. The formula is as follows:~~

$$Dis = R \times arccos(\cos(Lat_{pred})\cos(Lat_{obs}) \times cos(Lon_{pred} - Lon_{pred})$$
$$+ \sin(Lat_{obs}) \times \sin(Lat_{pred}))$$

~~Where R is the radius of the earth, Lat_{obs} and Lon_{real} are the actual latitude and longitude, and~~

~~Lat_{obs} and Lon_{pred} are the predicted latitude and longitude.~~

4 Results

Three types of recurrent neural networks (RNN, LSTM, GRU) are used to train samples with eight timestamps and 11 features selected by the random forest method, according to their importance; the results of analyzing 49 TCs in 2019–2021 are then evaluated. We set the value of the batch size to 64 and the epoch to 100 and found that the model performed best when the number of neurons in the hidden layer is set to 128; this was determined via experiments using different numbers of neurons in the hidden layer. Early stopping is used to prevent overfitting. When the performance of the model in the validation set begins to decline, training is stopped to avoid overfitting due to continued training.

~~Figure 4 shows the predicted latitudes and longitudes based on three RNNs in the following 6 h, 12 h,~~

~~18 h, 24 h, 48 h, and 72 h, and the results of all three networks within 24 h are all approximately~~

~~consistent with the real data. As the forecast time increases, the error accumulates.~~

323
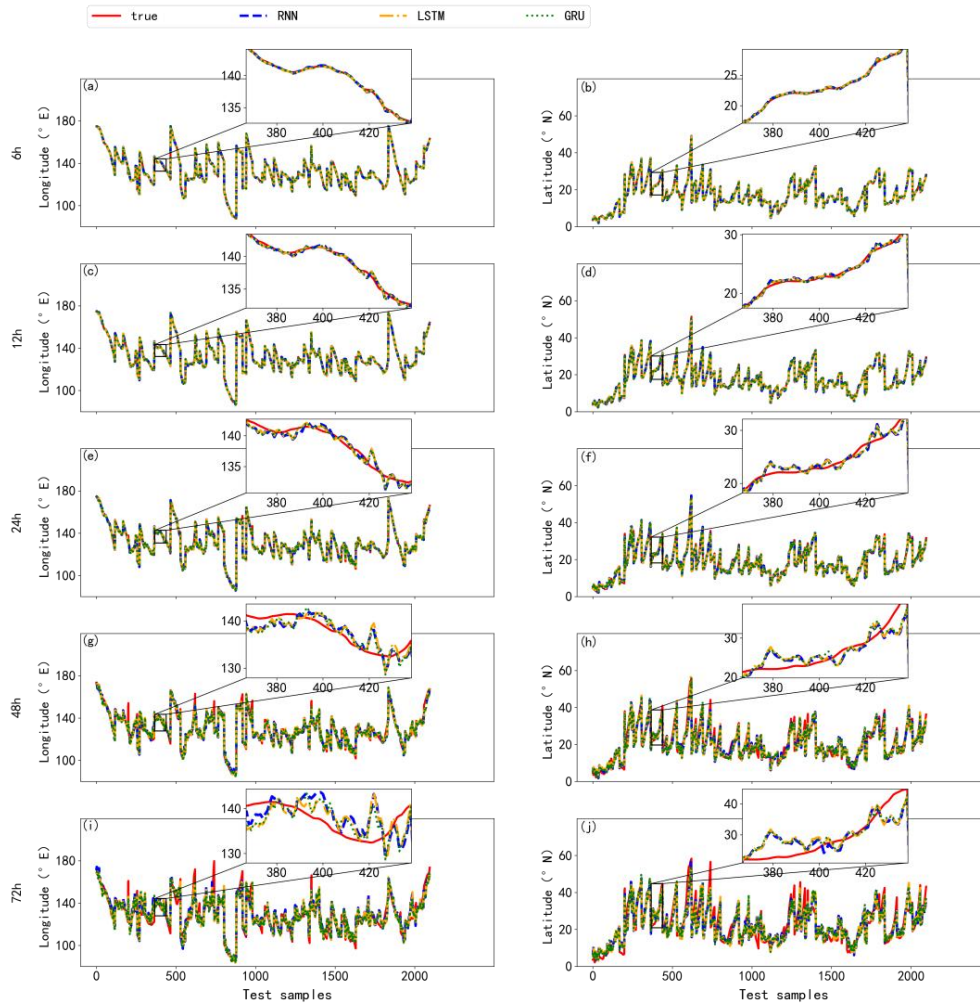
324 ~~Figure 4: Comparing the longitudes and latitudes of all test samples predicted by the three recurrent~~

325 ~~neural networks (RNN, LSTM, GRU), including the longitude/latitude forecasts at (a–b) 6 h, (c–d) 12 h,~~

326 ~~(e–f) 24 h, (g–h) 48 h, and (i–j) 72 h.~~

327

328 **Table 2~~1~~ Model performance evaluation (RMSE) for RNN, LSTM, and GRU**

Forecast Hour		Lat						Lon					
		6 h	12 h	18 h	24 h	48 h	72 h	6 h	12 h	18 h	24 h	48 h	72 h
Training Sets	RNN	0.146	0.368	0.624	0.912	2.232	4.069	0.153	0.412	0.735	1.118	3.181	6.236
	LSTM	0.126	0.335	0.584	0.867	2.34	3.986	0.149	0.391	0.703	1.077	3.232	6.172
	GRU	**0.112**	**0.312**	**0.555**	**0.83**	**2.282**	**3.883**	**0.134**	**0.376**	**0.681**	**1.041**	**3.152**	**6.031**
Validation Sets	RNN	0.171	0.441	0.76	1.116	2.723	4.493	0.182	0.483	0.865	1.337	3.739	6.715
	LSTM	0.157	0.428	0.751	1.103	**2.675**	**4.349**	0.183	**0.480**	**0.855**	**1.305**	3.69	6.761
	GRU	**0.157**	**0.42**	**0.735**	**1.086**	2.699	4.434	**0.179**	0.484	0.868	1.33	**3.632**	**6.608**
Test Sets	RNN	0.166	0.411	0.685	0.988	2.481	4.207	0.176	0.461	0.797	1.178	3.534	6.157
	LSTM	0.149	0.389	0.661	0.965	2.473	4.154	0.169	**0.456**	0.812	1.215	3.346	5.989
	GRU	**0.149**	**0.387**	**0.653**	**0.951**	**2.446**	**4.143**	**0.167**	0.457	**0.8**	**1.185**	**3.325**	5.969

329

The performance evaluation of the three RNN models is displayed in Table 1 by calculating the RMSE values between the predicted longitude (latitude) and the actual longitude (latitude), including training, validation, and test sets; the best results are highlighted in bold font. It is clear that the GRU-based and LSTM-based models significantly outperformed the RNN-based model, which suggests that the RNN is inferior in handling the problem of long-term dependence. GRU is a variant of LSTM that combines the forget and input gates in LSTM into an update gate and also merges the cell and hidden states. Hence, the parameter amounts of GRU are less than those of LSTM, which results in the overall training speed of GRU being faster than that of LSTM. GRU is theoretically similar to LSTM and can achieve the same accuracy as LSTM (or even better), so the results of GRU and LSTM are close and their RMSE values are much lower than that of RNN. GRU achieves the best performance in all forecast hours, with the smallest RMSE in the test set. Therefore we use GRU as a part of the fusion network model called GRU_CNN,adding meteorological environment data processed with CNN.

Table 322 Comparison of the average absolute distance errors (km) predicted by multiple deep-learning models

	6 h	12 h	18 h	24 h	48 h	72 h
CLIPER(Demaraia,1992)	—	—	—	213	442	659
BP	23.86	59.58	101.01	146.91	377.64	634.42
RNN	21.43	55.46	94.59	138.09	373.12	625.17
LSTM	19.65	52.38	91.76	136.05	360.32	614.76
GRU	19.51	52.6	91.21	134.73	357.25	607.44
NMSTN(Huang,2022)	27.52	59.09	—	139.18	336.16	544.16
GRU_CNN	**17.22**	**43.9**	**72.74**	**106.16**	**281.52**	**502.71**

Table 2 compares the results between GRU_CNN and various deep-learning models, showing the forecast results in the form of the mean absolute distance error. It is evident that GRU_CNN presents an absolute advantage in long-term forecasting. Both LSTM and GRU retain important features through various gate functions, which ensures that they will not be lost during long-term propagation. They can better predict the medium and long-term tracks of the TCs, compared with standard RNNs and two traditional methods named CLIPER and BP. The GRU_CNN is more accurate than the models without CNN. The average distance errors at 6 h, 24 h, 48 h, and 72 h are 17.22 km, 106.16 km, 281.52 km, and 502.71 km, respectively. The error is also reduced compared with the NMSTN method proposed by Huang et al. (2022). In addition, although there is a big difference between the long-term

354 forecast and the numerical prediction results, the average distance prediction results are better than the

355 results provided by the Central Meteorological Observatory (CMO) in the short-term forecasts,

356 including the 6 h (27.57 km) and 12 h (59.09 km) forecasts.

357

358
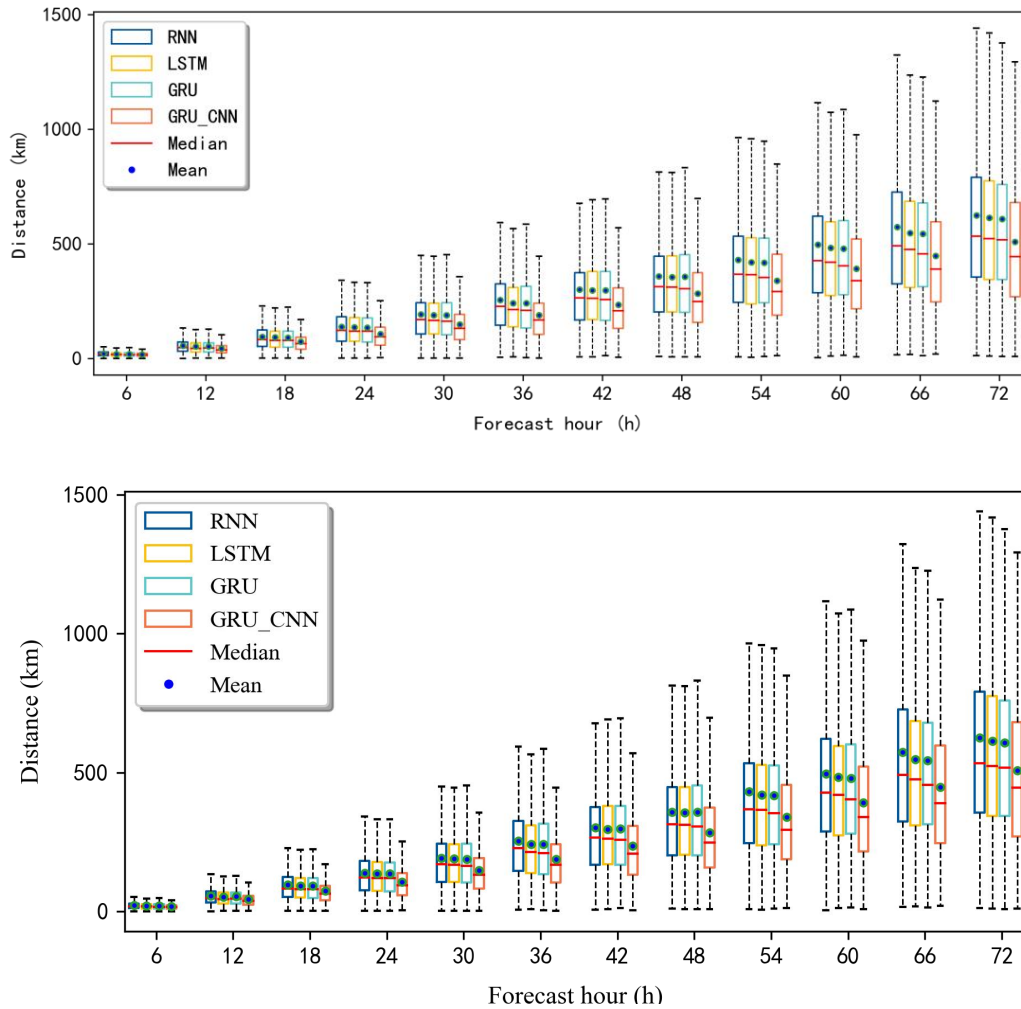
359 **Figure 355: The absolute average distance boxplot of the three kinds of recurrent neural networks (RNN,**

360 **LSTM, GRU) and the method in this paper (GRU_CNN) creating 6–72 h forecasts (interval 6 h).**

361 As shown in Fig. 5, the maximum distance errors predicted by the three RNNs at 48 h and 72 h are

362 over 500 km and 1000 km, respectively. Only considering the trajectory characteristics of the TCs in

363 the RNN while ignoring the external atmospheric environmental characteristics will cause instability in

364 the prediction of the TC tracks. The errors of the maximum and average values predicted by the

365 GRU_CNN model are both significantly reduced. To illustrate GRU_CNN more comprehensively and

366 intuitively, Fig. 6 shows a scatter plot of the predicted and actual values. The distance between the data

367   points and the diagonal line represents the prediction error. The higher the wind speed, the stronger the

368   intensity of the TCs, and the closer the predicted value is to the actual value. In addition, with the

369   increase in the forecast time, in high latitude and longitude forecasts when the TC is moving towards

370   the northwest, the predicted value is often lower than the actual value.

371

372
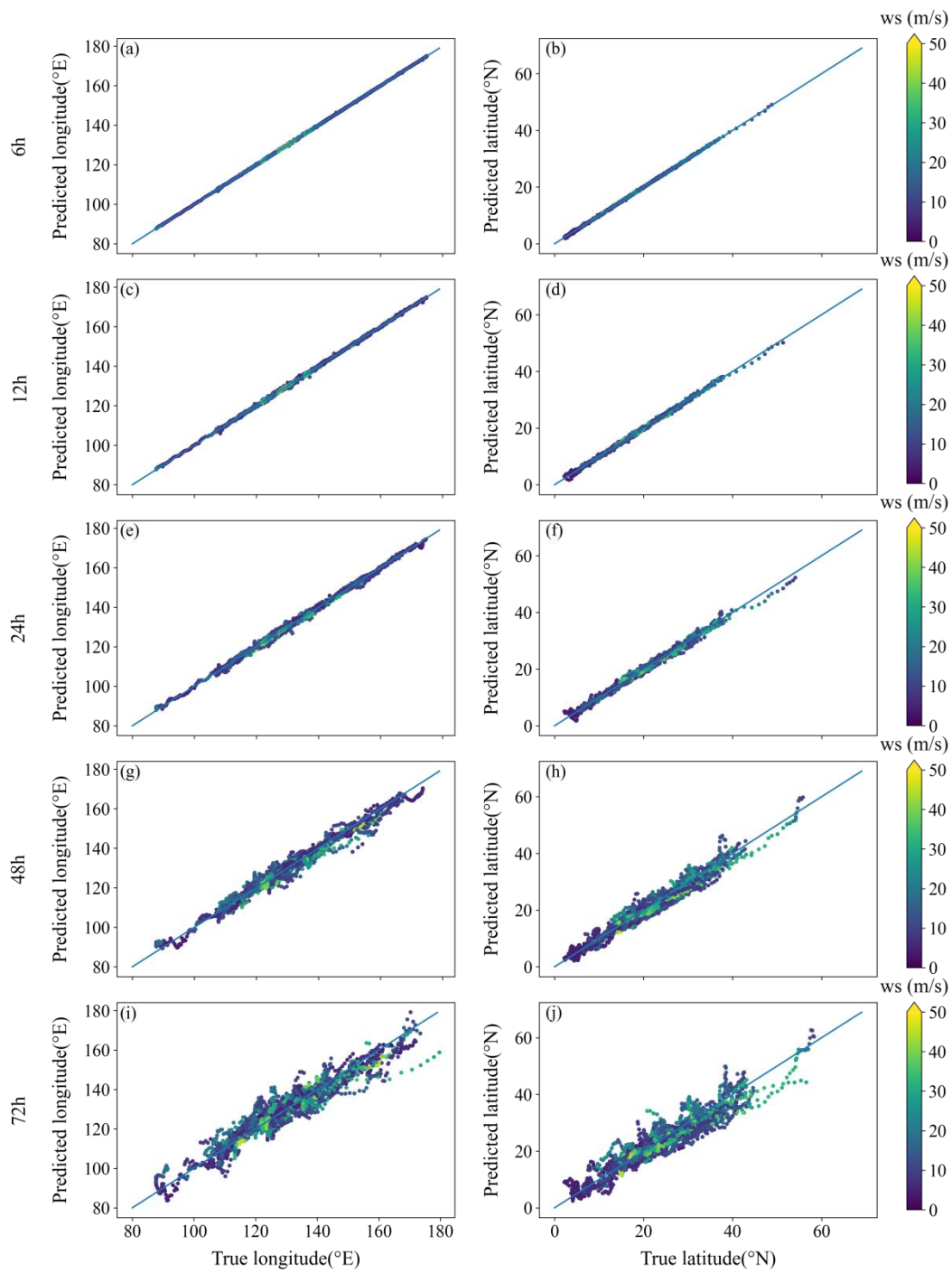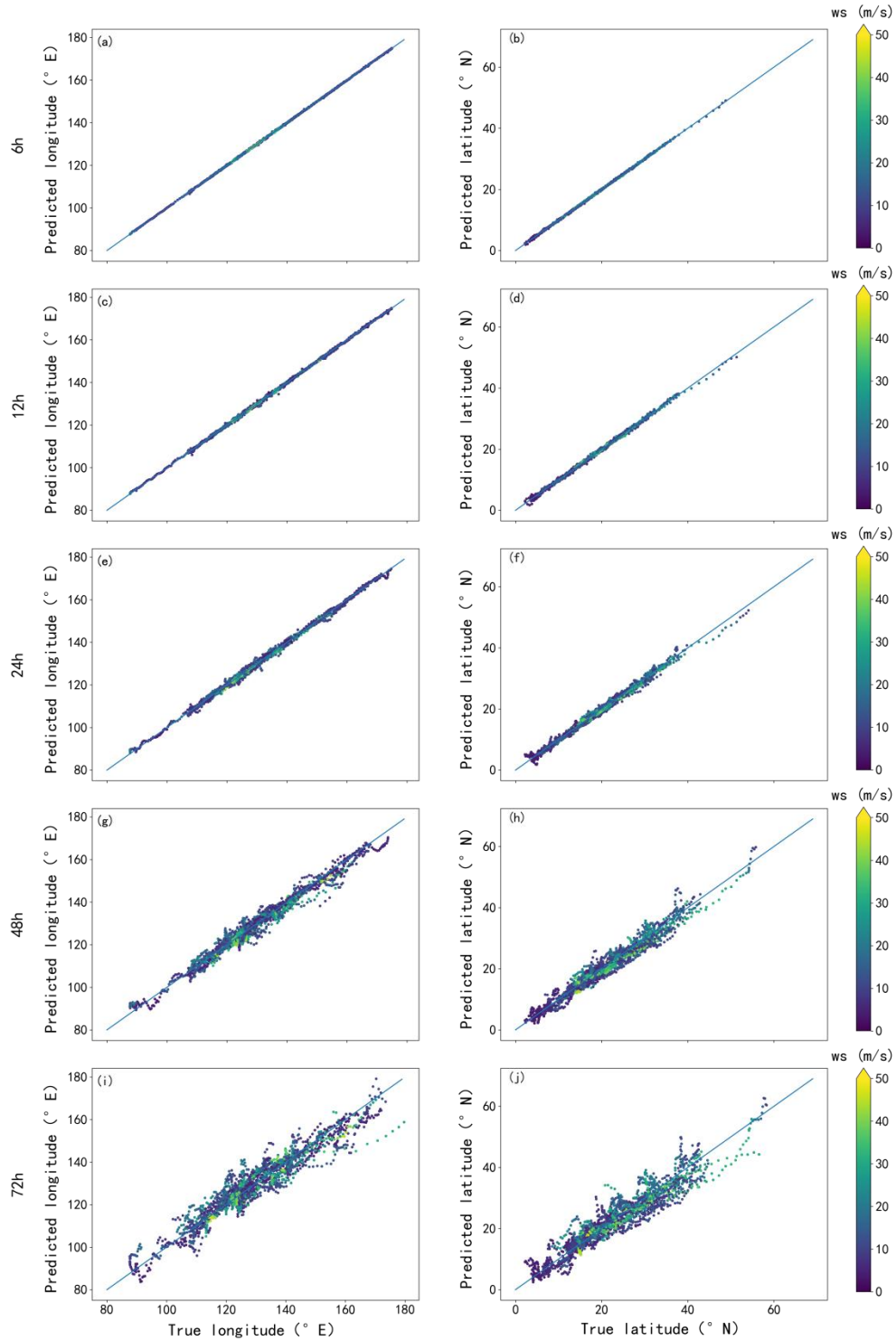
Figure 466: Scatter plot distributions of latitude predictions. The color bar represents the maximum wind speed, including the longitude and latitude forecasts at (a–b) 6 h, (c–d) 12 h, (e–f) 24 h, (g–h) 48 h, and (i–j) 72 h.

376   Data from three environmental fields are used in this paper: SST, geopotential height (pressure),

377   and wind field (*u*- and *v*-component) data. Different environmental input variables show different

378   effects in the model (Table 3). GRU+SST (pressure, UV) represents only the combination of the

379   trajectory characteristics and SST (geopotential height, wind field), while GRU+CNN is the result of

380   the fusion of the three. The results in Table 3 indicate that GRU+UV performed best, followed by

381   GRU+pressure and then GRU+SST, indicating that the steering flow plays a dominant role in TC

382   forecasting, especially in the short-term < 24-h forecast. The forecasting results of adding only the

383   steering flow are close to those of GRU_CNN, while the results at 48 h and 72 h illustrate that the

384   influence of the SST and geopotential height on the long-term TC forecast track gradually increases.

385   **Table 43 Comparison of trajectory data combining different environmental features. RMSE is the root**

386   **mean square error of latitude and longitude, and the distance is the average absolute distance error (km).**

	GRU+SST		GRU+Pressure		GRU+UV		GRU+CNN	
	RMSE	Distance (km)	RMSE	Distance (km)	RMSE	Distance (km)	RMSE	Distance (km)
6 h	0.154	19.35	0.132	16.15	0.137	16.94	0.138	17.22
12 h	0.419	52.37	0.352	44.22	0.347	43.74	0.35	43.9
18 h	0.739	92.25	0.598	76.16	0.575	72.81	0.575	72.74
24 h	1.103	137.78	0.883	112.93	0.841	106.63	0.837	106.16
48 h	2.858	358.25	2.462	306.03	2.379	302.76	2.248	281.52
72 h	4.913	588.08	4.52	557.86	4.385	524.88	4.146	502.71

387

388   To better show the model forecast of GRU_CNN, Figures 7–9 present the observed and forecast

389   tracks at 6 h and 24 h of TCs FAXAI, MITAG, and IN-FA, respectively, and the forecast tracks of

390   other TCs in the test set are presented in Supplementary Fig. S1-51. The blue lines represent the

391   observed tracks, while the red and yellow lines indicate the 6-h and 24-h forecast tracks. In general, it

392   is particularly hard to forecast unexpected turns in the TC track. The three TCs shown all exhibit a

393   sudden northward or northwestern turn in the TC track. For the 6-h forecast, the predicted path is

394   approximately consistent with the actual track, while the 24-h forecast has some deviations. The

395   average distance predicted near the northwest turn of FAXAI is 91.35 km; the error for MITAG's first

396   turn to the north is 127.02 km, and the error for the second turn to the northwest is 121.91 km. The two

397   average errors in the track forecast for In-fa are 84.27 km and 82.37 km. It can be seen that there is no

398   significant deviation in the forecast around the steering point, but, for some abnormal track changes,

399   such as crossing back over the same location, samples with more significant errors will be generated,

400   reducing the overall average absolute distance error.
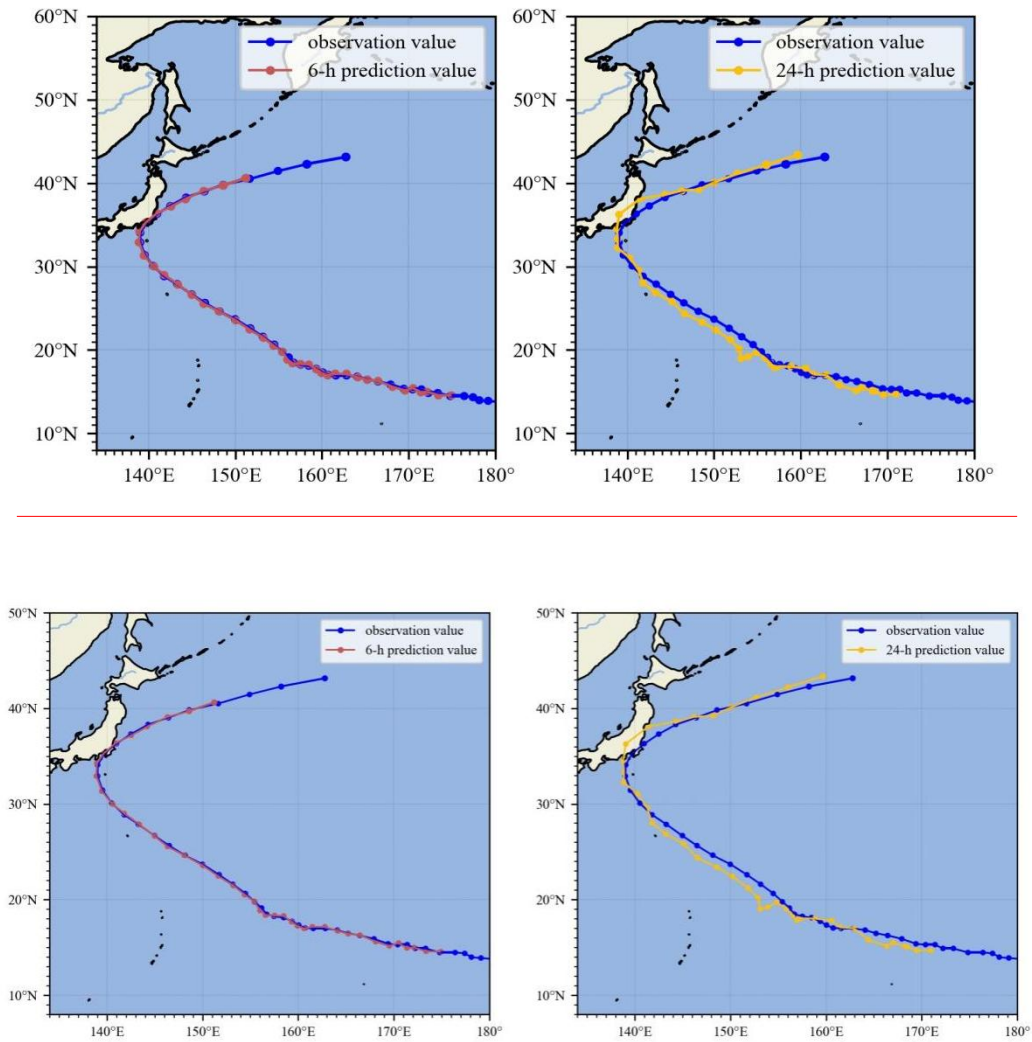
403   **Figure 577: Forecast tracks of Tropical Cyclone FAXAI (19152019) (left: 6 h, right: 24 h).**
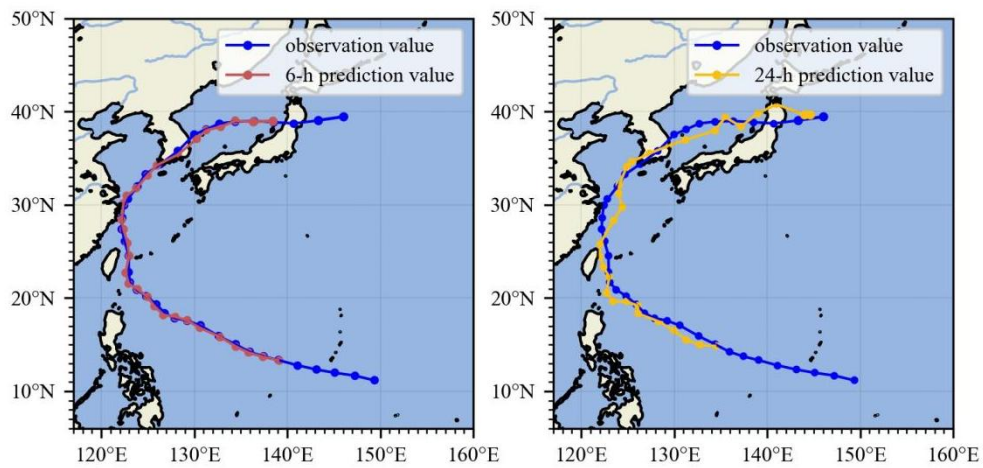
404
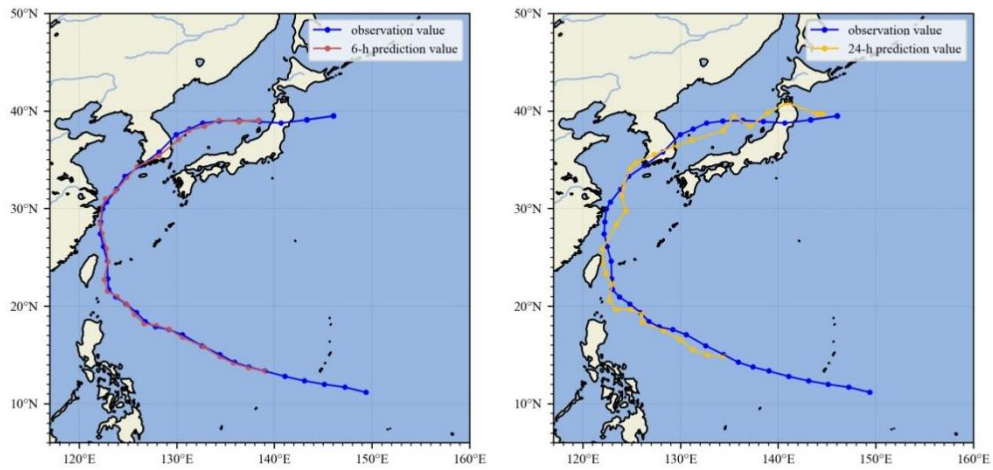
405

406   **Figure ~~6~~88: Forecast tracks of Tropical Cyclone MITAG (~~1918~~2019) (left: 6 h, right: 24 h).**

407

408
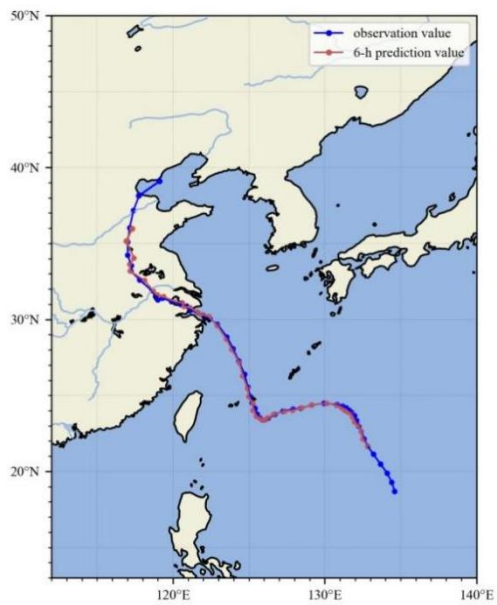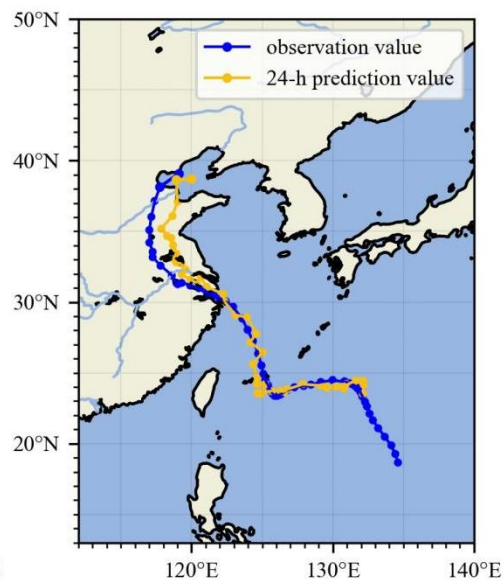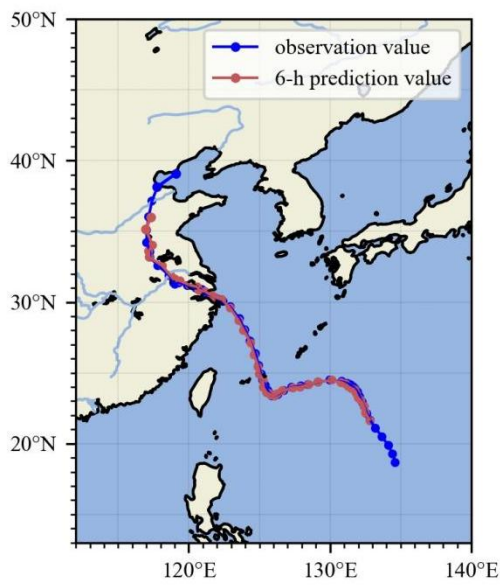
409   **Figure ~~799~~: Forecast tracks of Tropical Cyclone IN-FA (~~2106~~2021) (left: 6 h, right: 24 h).**

410   **5 Conclusion**

411   The past 24-h TC trajectory and meteorological field data have been used to forecast TC tracks in the

412   Northwest Pacific from hours 6–72 using deep learning methods. First, in order to eliminate data

413   redundancy and reduce the complexity of the prediction model, the random forest algorithm was used

414   for feature extraction of the two-dimensional movement data. Second, three kinds of recurrent neural

networks (RNN, LSTM, GRU) were used to evaluate and compare the models based on the input of trajectory features, and it was concluded that GRU performed relatively better in predicting TC tracks. Eventually, we combined GRU with CNN by adding the pre-processed meteorological environmental data around the cyclones (removing the vortex to obtain the steering flow); the CNN models the selected meteorological variables and extracts features, while GRU processes trajectory sequences. GRU_CNN has better prediction results than traditional single deep-learning methods do.

When a new TC generates in the ocean, the GRU_CNN model can quickly provide the forecast track within seconds. Short-term predictions within 12 h of initialization can provide better results than CMO can, and the average distance errors of the forecasts at 6 h and 12 h are 17.22 km and 43.9 km. When the forecast goes beyond 24 h, the model's accuracy declines. The historical steering flow of cyclones has a significant effect on improving the accuracy of short-term forecasting, while, in long-term forecasting, the SST and geopotential height will have a particular impact, which is regarded as a crucial way to expand and improve the application of deep-learning models in TC track forecasting, In addition, the model can accurately predict TCs that suddenly turn to the north or northwest, but there will be a considerable distance error for abnormal trajectories, possibly due to a lack of synoptic analysis in our study.

Cyclone prediction has been a challenge in weather forecasting for a long time. With future scientific and technological advances, it is becoming increasingly convenient to obtain meteorological data, and the database has gradually expanded. At the same time, deep-learning models are flexible and can easily be expanded upon. In the future, more data can be integrated, and more valuable features can be extracted to improve the prediction accuracy of the deep-learning model. In addition, model predictor variables will be considered in future work, the inclusion of which can predict more useful information, such as cyclone intensity, rainfall, and wind speed.

Code availability. The code and model are available as a free access repository on GitHub at https://zenodo.org/record/7454324#.Y58Dwv3P2Uk~~https://github.com/Hush980/TCs_DL_code~~.

Data availability. IBTrACS that we used in this study is publicly available. It can be down-loaded at https://www.ncei.noaa.gov/data/international-best-track-archive-for-climate-stewardship-ibtracs/v04r0

0/access/netcdf/IBTrACS.WP.v04r00.nc. ERA5 data can be obtained from Copernicus Climate Data Store (https://cds.climate.copernicus.eu).

Author contributions. Liang Wang wrote the paper and conducted most of the code implementation and data analysis. Bincheng Wan designed the research framework. Shaohui Zhou provided the code and revised the paper. Haofei Sun was involved in data collation and Zhiqiu Gao was responsible for supervision.

Competing interests. The authors declare that they have no known competing financial interests or personal relationships that could have appeared to influence the work reported in this paper.

Acknowledgments. This study was supported by the National Key Research and Development Program of the Ministry of Science and Technology of China (2018YFC1506405), and by the National Natural Science Foundation of China (Grants 42175082 and 42222503). We are very grateful to anonymous reviewers for their careful review and valuable comments, which led to substantial improvement of this manuscript.

References

Alemany, S., Beltran, J., Perez, A., and Ganzfried, S.: Predicting Hurricane Trajectories Using a Recurrent Neural Network, Proceedings of the AAAI Conference on Artificial Intelligence, 33, https://doi.org/10.1609/aaai.v33i01.3301468, 2018.

Ali, M. M., Kishtawal, C. M., and Jain, S.: Predicting cyclone tracks in the north Indian Ocean: An artificial neural network approach, Geophysical Research Letters, 34, https://doi.org/10.1029/2006gl028353, 2007.

Bathla, G.: Stock Price prediction using LSTM and SVR, 2020 Sixth International Conference on Parallel, Distributed and Grid Computing (PDGC), 6-8 Nov. 2020, 211-214, https://doi.org/10.1109/PDGC50313.2020.9315800,

465 Boussioux, L., Zeng, C., Guenais, T., and Bertsimas, D.: Hurricane Forecasting: A Novel Multimodal

466   Machine Learning Framework, Weather and Forecasting, https://arxiv.org/abs/2011.06125, 2022.

467 Brand, S., Buenafe, C. A., and Hamilton, H. D.: Comparison of Tropical Cyclone Motion and

468   Environmental Steering, Monthly Weather Review, 109, 908-909,

469   https://doi.org/10.1175/1520-0493(1981)109<0908:cotcma>2.0.co;2, 1981.

470 Chan, J. and Kepert, J.: Global Perspectives on Tropical Cyclones: From Science to Mitigation,

471   https://doi.org/10.1142/7597, 2010.

472 Chan, J. C.-L.: An Observational Study of the Physical Processes Responsible for Tropical Cyclone

473   Motion, Journal of Atmospheric Sciences, 41, 1036-1048,

474   https://doi.org/10.1175/1520-0469(1984)041<1036:aosotp>2.0.co;2, 1984.

475 Chan, J. C. L., Gray, W. M., and Kidder, S. Q.: Forecasting Tropical Cyclone Turning Motion from

476   Surrounding Wind and Temperature Fields, Monthly Weather Review, 108, 778-792,

477   https://doi.org/10.1175/1520-0493(1980)108<0778:FTCTMF>2.0.CO;2, 1980.

478 Cho, K., Merriënboer, B. v., Gulcehre, C., Bahdanau, D., Bougares, F., Schwenk, H., and Bengio, Y.:

479   Learning Phrase Representations using RNN Encoder--Decoder for Statistical Machine

480   Translation, In Proceedings of the 2014 Conference on Empirical Methods in Natural Language

481   Processing (EMNLP), https://doi.org/10.3115/v1/D14-1179, 2014.

482 Díaz-Uriarte, R. and Alvarez de Andrés, S.: Gene selection and classification of microarray data using

483   random forest, BMC bioinformatics, 7, 3, https://doi.org/10.1186/1471-2105-7-3, 2006.

484 Emanuel, K.: Will Global Warming Make Hurricane Forecasting More Difficult?, Bulletin of the

485   American Meteorological Society, 98, 495-501, https://doi.org/10.1175/bams-d-16-0134.1, 2017.

486 Galarneau, T. J. and Davis, C. A.: Diagnosing Forecast Errors in Tropical Cyclone Motion, Monthly

487   Weather Review, 141, 405-430, https://doi.org/10.1175/mwr-d-12-00071.1, 2013.

488 Gao, S., Zhao, P., Pan, B., Li, Y., Zhou, M., Xu, J., Zhong, S., and Shi, Z.: A nowcasting model for the

489   prediction of typhoon tracks based on a long short term memory neural network, Acta

490   Oceanologica Sinica, 37, 8-12, https://doi.org/10.1007/s13131-018-1219-z, 2018.

491 Genuer, R., Poggi, J.-M., and Tuleau-Malot, C.: Variable selection using random forests, Pattern

492   Recognition Letters, 31, 2225-2236, https://doi.org/10.1016/j.patrec.2010.03.014, 2010.

493 George, J. E. and Gray, W. M.: Tropical Cyclone Motion and Surrounding Parameter Relationships,

494   Journal of Applied Meteorology and Climatology, 15, 1252-1264,

495   https://doi.org/10.1175/1520-0450(1976)015<1252:TCMASP>2.0.CO;2, 1976.

496 Giffard-Roisin, S., Yang, M., Charpiat, G., Kégl, B., and Monteleoni, C.: Fused Deep Learning for

497   Hurricane Track Forecast from Reanalysis Data, Climate Informatics Workshop Proceedings 2018,

498   Boulder, United States, 2018-09-19, https://hal.science/hal-01851001, 2018.

499 Giffard-Roisin, S., Yang, M., Charpiat, G., Kumler Bonfanti, C., Kégl, B., and Monteleoni, C.:

500   Tropical Cyclone Track Forecasting Using Fused Deep Learning From Aligned Reanalysis Data,

501   Front Big Data, 3, 1, https://doi.org/10.3389/fdata.2020.00001, 2020.

502 Goerss, J. S.: Tropical Cyclone Track Forecasts Using an Ensemble of Dynamical Models, Monthly

503   Weather Review, 128, 1187-1193,

504   https://doi.org/10.1175/1520-0493(2000)128<1187:tctfua>2.0.co;2, 2000.

505 Goldenberg, S. B., Landsea, C. W., Mestas-Nuñez, A. M., and Gray, W. M.: The Recent Increase in

506   Atlantic Hurricane Activity: Causes and Implications, Science, 293, 474-479,

507   https://doi.org/doi:10.1126/science.1060040, 2001.

508 Graves, A., Jaitly, N., and Mohamed, A.: Hybrid speech recognition with Deep Bidirectional LSTM,

509   2013 IEEE Workshop on Automatic Speech Recognition and Understanding, 8-12 Dec. 2013,

510   273-278, https://doi.org/10.1109/ASRU.2013.6707742,

511 Gray, W. M.: Global View of the Origin of Tropical Disturbances and Storms, Monthly Weather

512   Review, 96, 669-700, http://dx.doi.org/10.1175/1520-0493(1968)096<0669:GVOTOO>2.0.CO;2,

513   1968.

514 Hochreiter, S. and Schmidhuber, J.: Long short-term memory, Neural computation, 9, 1735-1780,

515   https://doi.org/10.1162/neco.1997.9.8.1735, 1997.

516 Holland, G. J.: Tropical Cyclone Motion: Environmental Interaction Plus a Beta Effect, Journal of the

517   Atmospheric Sciences, 40, 328-342,

518   https://doi.org/10.1175/1520-0469(1983)040<0328:tcmeip>2.0.co;2, 1983.

519 Holland, G. J.: Tropical Cyclone Motion. A Comparison of Theory and Observation, Journal of

520   Atmospheric Sciences, 41, 68-75,

521   https://doi.org/10.1175/1520-0469(1984)041<0068:tcmaco>2.0.co;2, 1984.

522   Huang, C., Bai, C., Chan, S., and Zhang, J.: MMSTN: A Multi-Modal Spatial-Temporal Network for

523   Tropical Cyclone Short - Term Prediction, Geophysical Research Letters, 49,

524   https://doi.org/10.1029/2021gl096898, 2022.

525   Ioffe, S. and Szegedy, C.: Batch Normalization: Accelerating Deep Network Training by Reducing

526   Internal Covariate Shift, Proceedings of the 32nd International Conference on International

527   Conference on Machine Learning, 37, 448-456, https://doi.org/10.48550/arXiv.1502.03167, 2015.

528   Katsube, K. and Inatsu, M.: Response of Tropical Cyclone Tracks to Sea Surface Temperature in the

529   Western North Pacific, Journal of Climate, 29, 1955-1975,

530   https://doi.org/10.1175/jcli-d-15-0198.1, 2016.

531   Kim, S., Kang, J.-S., Lee, M., and Song, S.-k.: DeepTC: ConvLSTM Network for Trajectory Prediction

532   of Tropical Cyclone using Spatiotemporal Atmospheric Simulation Data, In Spatiotemporal

533   Workshop at 31st Conference on Neural Information Processing Systems, 2018.

534   Kitade, T.: A Numerical Study of the Vortex Motion with Barotropic Models, Journal of the

535   Meteorological Society of Japan. Ser. II, 59, 801-807, https://doi.org/10.2151/jmsj1965.59.6_801,

536   1981.

537   Klein, B., Wolf, L., and Afek, Y.: A Dynamic Convolutional Layer for short rangeweather prediction,

538   2015 IEEE Conference on Computer Vision and Pattern Recognition (CVPR), 7-12 June 2015,

539   4840-4848, https://doi.org/10.1109/CVPR.2015.7299117,

540   Krizhevsky, A., Sutskever, I., and Hinton, G.: ImageNet Classification with Deep Convolutional

541   Neural Networks, Neural Information Processing Systems, 25, https://doi.org/10.1145/3065386,

542   2012.

543   Lecun, Y., Bottou, L., Bengio, Y., and Haffner, P.: Gradient-Based Learning Applied to Document

544   Recognition, Proceedings of the IEEE, 86, 2278-2324, https://doi.org/10.1109/5.726791, 1998.

545   Li-min, S., Gang, F. U., Xiang-chun, C., and Jian, Z.: Application of BP neural network to forecasting

546   typhoon tracks, Journal of Natural Disasters, 18, 104-111,

547   https://doi.org/0.3969/j.issn.1004-4574.2009.06.018, 2009.

548   Liu, H., Mi, X., and Li, Y.: Smart multi-step deep learning model for wind speed forecasting based on

549   variational mode decomposition, singular spectrum analysis, LSTM network and ELM, Energy

550   Conversion and Management, 159, 54-64, https://doi.org/10.1016/j.enconman.2018.01.010, 2018.

551 Liu, Z., Hao, K., Geng, X., Zou, Z., and Shi, Z.: Dual-Branched Spatio-Temporal Fusion Network for

552   Multihorizon Tropical Cyclone Track Forecast, IEEE Journal of Selected Topics in Applied Earth

553   Observations and Remote Sensing, 15, 3842-3852, https://doi.org/10.1109/JSTARS.2022.3170299,

554   2022.

555 Lownam, C.: The NCAR-AFWA tropical cyclone bogussing scheme. A report prepared for the Air

556   Force Weather Agency (AFWA), National Center for Atmospheric Research, 2001.

557 Moradi Kordmahalleh, M., Gorji Sefidmazgi, M., Homaifar, A., and Liess, S.: Hurricane Trajectory

558   Prediction Via a Sparse Recurrent Neural Network,   2015.

559 NEUMANN, C. J. and HOPE, J. R.: Performance Analysis of the HURRAN Tropical Cyclone

560   Forecast   System,   Monthly   Weather   Review,   100,   245-255,

561   https://doi.org/10.1175/1520-0493(1972)100<0245:paotht>2.3.co;2, 1972.

562 Ortega, L. C., Otero, L. D., Solomon, M., Otero, C. E., and Fabregas, A.: Deep learning models for

563   visibility   forecasting   using   climatological   data,   International   Journal   of   Forecasting,

564   https://doi.org/10.1016/j.ijforecast.2022.03.009, 2022.

565 Roy, C. and Kovordányi, R.: Tropical cyclone track forecasting techniques — A review, Atmospheric

566   Research, 104-105, 40-69, https://doi.org/10.1016/j.atmosres.2011.09.012, 2012.

567 Ruttgers, M., Lee, S., Jeon, S., and You, D.: Prediction of a typhoon track using a generative

568   adversarial   network   and   satellite   images,   Sci   Rep,   9,   6057,

569   https://doi.org/10.1038/s41598-019-42339-y, 2019.

570 Schulthess, T. C., Bauer, P., Wedi, N., Fuhrer, O., Hoefler, T., and Schär, C.: Reflecting on the Goal

571   and Baseline for Exascale Computing: A Roadmap Based on Weather and Climate Simulations,

572   Computing in Science & Engineering, 21, 30-41, https://doi.org/10.1109/MCSE.2018.2888788,

573   2019.

574 Shi, X., Chen, Z., Wang, H., Yeung, D.-Y., Wong, W. K., and Woo, W.-c.: Convolutional LSTM

575   Network: A Machine Learning Approach for Precipitation Nowcasting, Proceedings of the 28th

576   International   Conference   on   Neural   Information   Processing   Systems,   1,   802-810,

577   https://doi.org/10.48550/arXiv.1506.04214, 2015.

578 Sun, Y., Zhong, Z., Li, T., Yi, L., Camargo, S. J., Hu, Y., Liu, K., Chen, H., Liao, Q., and Shi, J.:

579   Impact of ocean warming on tropical cyclone track over the western north pacific: A numerical

investigation based on two case studies, Journal of Geophysical Research: Atmospheres, 122, 8617-8630, https://doi.org/10.1002/2017JD026959, 2017.

Wang, C. and Fu, Y.: Ship Trajectory Prediction Based on Attention in Bidirectional Recurrent Neural Networks, 529-533, https://doi.org/10.1109/isctt51595.2020.00100, 2020.

Wang, Y., Zhang, W., and Fu, W.: Back Propogation(BP)-neural network for tropical cyclone track forecast, Proceedings - 2011 19th International Conference on Geoinformatics, Geoinformatics 2011, 1-4, https://doi.org/10.1109/GeoInformatics.2011.5981095, 2011.

Zhang, Y., Chandra, R., and Gao, J.: Cyclone Track Prediction with Matrix Neural Networks, 2018 International Joint Conference on Neural Networks (IJCNN), 1-8, https://doi.org/10.1109/IJCNN.2018.8489077, 2018.